2019-12-01

Electrical Conductivity of the Aluminum Oxide Diffusion Barrier Following Catalytic Carbon Nanotube Growth

Berg Daniel Dodson
Brigham Young University

Electrical Conductivity of the Aluminum Oxide Diffusion Barrier Following Catalytic Carbon Nanotube Growth

Berg Daniel Dodson

A thesis submitted to the faculty of
Brigham Young University
in partial fulfillment of the requirements for the degree of

Master of Science

Richard R. Vanfleet, Chair
Robert C. Davis
Brian D. Jensen

Department of Physics and Astronomy

Brigham Young University

ABSTRACT

Electrical Conductivity of the Aluminum Oxide Diffusion Barrier
Following Catalytic Carbon Nanotube Growth

Berg Daniel Dodson
Department of Physics and Astronomy, BYU
Master of Science

Carbon nanotube templated microfabrication (CNT-M) is a method that allows high-aspect ratio structures to be made for microelectromechanical systems (MEMS) devices. One concern when making monolithic electrical devices using CNT-M is that the aluminum oxide diffusion barrier will create too large of a resistance in the device. However, in developing CNT based MEMS devices, it has been observed that an electrical DC current is capable of transport from a conductive substrate, across the aluminum oxide, and through to the CNT structure grown on top of it. This thesis attempts to determine the mechanisms responsible for current being able to cross the aluminum oxide diffusion barrier easily through sample characterizations. Principally, current-voltage measurements, electron microscopy, XEDS, and SIMS analysis are used to characterize the various samples and determine the process responsible for the observed phenomenon. Through these techniques, it is determined exposure to ethylene gas during the CNT growth recipe used in our lab, regardless of whether CNTs grow on the sample or not, is necessary to cause a drop in resistance across the aluminum oxide, but the that the overall content of iron and carbon in the aluminum oxide do not correlate with this drop in resistance.

Keywords: aluminum oxide, carbon nanotubes, diffusion barrier

ACKNOWLEDGMENTS

I would like to thank all the people responsible for bringing this graduate thesis to fruition. This thesis is the culmination of no one individual, but is the result of the work, collaboration, and longsuffering of many.

To my graduate committee, Dr. Vanfleet, Dr. Davis, and Dr. Jensen, I thank you for being the true teachers while I was working on this thesis. It was the courses you taught, the expectations you set, and pointing me in the right direction when I felt stymied that help grow over the course of this project. I thank you for your flexibility and involvement in spite of an unending list of responsibilities, unforeseeable inconveniences, and demands on your time by countless more intriguing opportunities. Working with you was empowering.

To the faculty and staff in charge of research facilities, I thank you for your training. Without you imparting your expertise I never could have completed even the least part of the work that went into this thesis. Thank you for your work in maintaining all of the equipment. My peak behind the curtain of how needy and temperamental equipment can be, especially when treated wrong, has given me an unending appreciation of all the work that keeps these machines up and running.

I would finally like to thank my family, both immediate and extended, for humoring me with their nods and encouragement as I would attempt to explain to them something even I didn't fully understand at the time. I would like thank them for their understanding as I would change plans last minute with the only explanation given being "Sorry, I have work to do." I would like to thank them for providing the support necessary to survive a graduate program.

TABLE OF CONTENTS

LIST OF FIGURES

Chapter 1 – Introduction

1.1 CNT MEMS

Carbon nanotube-templated microfabrication (CNT-M) is a recent development in microelectromechanical systems (MEMS) fabrication. The focus of CNT-M is to create MEMS devices by creating patterned carbon nanotube (CNT) structures in conjunction with standard microfabrication techniques[1]. These 3D CNT structures make it possible to take advantage of the intrinsic properties of CNTs in MEMS applications.

The properties that make CNTs so attractive for MEMS development include their mechanical, electrical, and structural properties. With a Young's modulus reported as between 270 GPa and 3.6 TPa[2–4] CNTs are a robust material that can be used to strengthen structures. CNTs also exhibit electrical conductivity or semiconductivity depending on the structure of the nanotubes[4–6]. Being thermally conductive is another advantage of CNTs[7,8]. Large void space between CNTs creates a structure that has a large surface area that can be used in many applications. High aspect ratio structures on the order of 250:1 are capable of being made from CNTs, too, creating structures with aspect ratios comparable to aspect ratios attained with LIGA[9].

The importance of these properties becomes apparent when the wide array of applications CNT-M is used for is considered. CNT-M has been used to fabricate compliant mechanisms[10,11], supercapacitors[12], micro-resonators[13,14], electrodes and microelectrode arrays[15–17]. By infiltrating the void space between the CNTs it is possible to tune final properties of the device being made. Metals such as copper or nickel have been used to fill the void space in the CNT structure through electroplating[18–20]. Other metals and non-metals, such as aluminum oxide, silica, and carbon, have been used to infiltrate the structure through atomic layer deposition[21–24] or chemical vapor infiltration[25–28]. By filling the void space in the CNT forest with other material, the whole structure

begins to take on the properties comparable to the properties of the bulk infiltrating material while retaining the unique 3D shape of the nanotube structure.

To be able to create CNT devices, though, the substrate needs to be prepared for CNT growth by deposition of two thin films. The first thin film to be deposited is the diffusion barrier and will be discussed in section 1.2. The second layer is the catalyst. These catalysts can be iron, cobalt, nickel, gold, lead, as well as other materials or transition metals[29,30]. Depending on the catalyst chosen, the method used to deposit the catalyst[31], and the amount of catalyst deposited[32], the resulting CNTs will take on different electrical properties, mechanical properties, levels of crystallinity in the CNTS as well as determine what temperatures CNTs grow at, if at all[29,33,34]. When choosing a catalyst for CNT-M processes, the following characteristics are important: CNT growth rate, areal density of nanotubes, ultimate height attainable, and resulting properties of the nanotubes. It is important to consider these factors when choosing a catalyst for growing CNTs, but iron is generally used for CVD CNT growth at BYU since it yields overall favorable results in these categories[33] as well as for the ease of deposition in our on-site thermal evaporator.

1.2 The Diffusion Barrier

The CNT-M paradigm wouldn't function without a diffusion barrier between the CNT catalyst and the substrate. The purpose of the diffusion barrier is to prevent catalyst diffusing into[35], alloying with, or forming a silicide[36] with the substrate during the growth process, all three of which would terminate CNT growth[35,37,38]. However, the diffusion barrier helps prevent the catalyst from interacting with substrate and thus helping to promote CNT growth. The diffusion barrier also contributes to CNT growth through catalyst-substrate interactions[39] that help to limit iron diffusion across the surface of the samples[40] helping the catalyst to form nanoparticles of an

appropriate size for CNT growth. The magnitude of these effects depend on the catalyst and diffusion barrier being used.

There are several materials that can be used as diffusion barriers for CNT growth. Some common diffusion barriers include aluminum oxide[40–42], silicon oxide[40], titanium oxide[41,42], and titanium nitride[41,42]. All of these diffusion barriers interact differently with the catalyst and produce CNT forests with different properties as a result. While comparing aluminum oxide to the titanium oxide and titanium nitride diffusion barriers it is seen that the growth rate of CNTs grown on aluminum oxide far exceeds that of CNTs grown on the other diffusion barriers[41]. Additionally, CNTs grown on aluminum oxide with an iron catalyst form CNT forests composed of CNTs with small diameters that were more closely packed than on other diffusion barriers, aiding CNT alignment overall. This is corroborated by the works of other groups[40] and is the reason that aluminum oxide is used in CNT-M.

One concern of using a diffusion barrier is that it makes it more difficult to electrically connect to the substrate[35]. In the case of aluminum oxide this is due in part to its resistivity: $\rho > 10^{14}\ \Omega\cdot cm$ for bulk aluminum oxide[43]. Attempts have been made to create CNT structures that are electrically connected to the substrate by thinning or removing the diffusion barrier[44,45], or using conductive diffusion barriers[46–48]. However, gaining conductivity in the CNT-M device by thinning or removing the aluminum oxide or choosing a different material for the diffusion barrier reduces the quality of CNT growths for the device.

1.3 When an Insulator Conducts Electricity: Changes in Conductivity

CNT structures grown on aluminum oxide don't seem to be electrically isolated from the substrate, though. Evidence for this can be found in monolithically fabricated, CNT based field emitters[44,49–51]. These CNT field emitters that were grown on an aluminum oxide diffusion barrier

were capable of supplying a constant current for an extended period of time. The implications of this are subtle; in order to supply a steady current, the electrons that were leaving the CNTs had to be replaced, suggesting that there is an electrical connection with the substrate. A similar phenomenon is seen in neural probes with CNT electrodes that were being developed at BYU. After growing CNT electrodes on 50 nm of aluminum oxide, current-voltage (I-V) measurements were made between the conductive substrate beneath the diffusion barrier and the CNTs on top of the diffusion barrier. These measurements indicated the resistance from the substrate to the top of the CNTs was 580 Ω on average[52].

This is especially interesting since prior to growth, the aluminum oxide layer exhibits a large electrical resistance. This can be seen in I-V measurements shown in figure 1. The curves seen in Figure 1 show current flow through the aluminum oxide layer as a function of applied voltage while increasing and then decreasing the applied voltage. When the aluminum oxide is first deposited on the tungsten, as in figure 1.a, there is no linear correlation between voltage and measured current response as would be expected in an ohmic sample. When the measurement is repeated after CNT growth, as seen in 1.b, even at one tenth of the potential, the current's response is at least 10^6 times larger and ohmic.

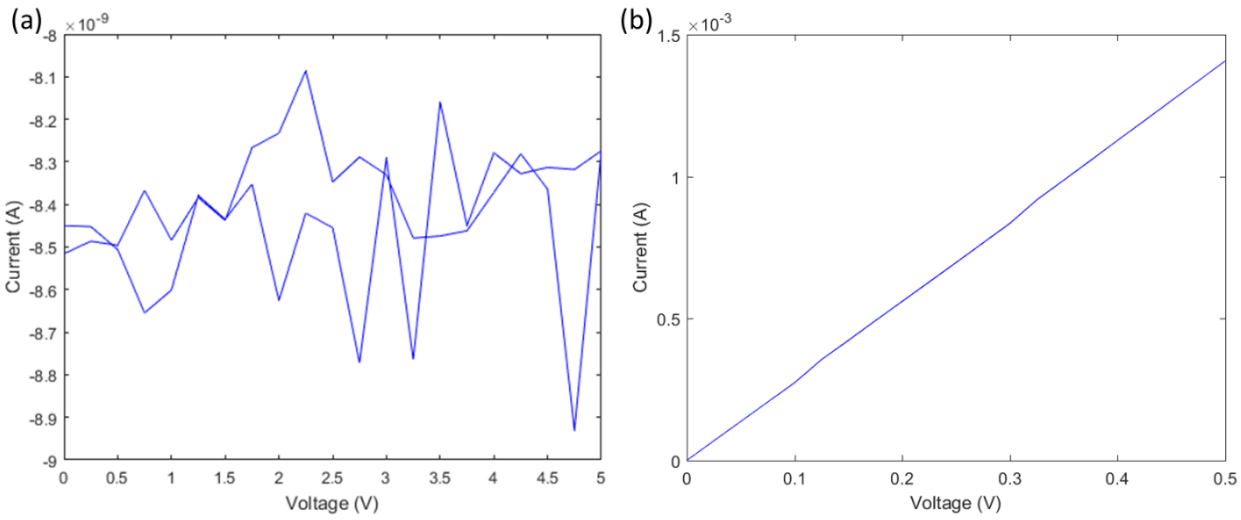

Figure 1. I-V measurements of the current passing across the aluminum oxide diffusion barrier in (a) a sample that has not been furnace processed and (b) a sample that had CNTs grown on it. Measurements made prior to CNT growth only show the nanoamp noise picked up by the detector. When one-tenth the voltage that was applied to sample prior to nanotube growth is applied to the sample after CNT growth almost 1.5 mA is detected.

In groups that have observed this phenomenon, the explanation that is used is that the microstructure of the aluminum oxide facilitates the diffusion of iron into the aluminum oxide[53,54]. This seems to be a plausible model since it is documented that as CNT growth occurs, the catalyst will diffuse into diffusion barrier[55].

1.4 Overview

The purpose of this Master's thesis was to understand this electrical conductivity transformation in the aluminum oxide diffusion barrier. This was done using samples with a conductive substrate covered by an aluminum oxide diffusion barrier. Samples with and without iron CNT catalyst deposited on the diffusion barrier were subjected to furnace treatments and CNT growth conditions. Average resistances of all these samples were collected by performing current-voltage measurements. Additional experiments including STEM imaging, XEDS, and SIMS were performed to better understand the mechanisms responsible for the changing conductivity.

Chapter 2 – Experimental

All experiments were performed on 15×15 mm^2 silicon dies coated with, in the order they were deposited on the wafer, 50 nm of aluminum oxide, 100 nm of tungsten, and 50 nm of aluminum oxide. The preparation of these samples and any modifications to these samples for the purposes of experimentation and analysis are discussed in the following sections.

2.1 – Basic Wafer Preparation

Silicon wafers were initially coated with 50 nm of aluminum oxide which was deposited on the wafers using a Denton Integrity 20 Coating System Vacuum E-beam Evaporator while the thickness was controlled using a crystal monitor. An 11-minute deposition of tungsten was done in a Kurt J. Lesker PVD 75 sputtering system, depositing 100 nm of tungsten. Two parallel stripes of an acetone soluble polymer, Sharpie marker, were applied to the surface of the tungsten. These stripes were separated from each other by 5 mm. Another aluminum oxide deposition was performed, creating a 50 nm thick diffusion barrier of aluminum oxide on top of the tungsten. This completed the thin film deposition for samples.

To turn the wafers into the sample dies, 50 drops of AZ 3330 photoresist was spun onto wafers at 5000 RPM for 1 minute. The wafer was then soft baked on a 90 °C hotplate for 1 minute. The wafers were diced into 15×15 mm^2 dies on a Disco DAD 320 dicing saw. The photoresist was removed by agitating samples in a 1-Methyl-2-pyrrolidinone (NMP) bath for 20 minutes. This NMP bath also dissolved the sharpie stripes, leaving behind exposed stripes of tungsten. Sample dies were placed in an isopropyl alcohol bath for 20 minutes, washed with deionized water and blown dry with nitrogen.

2.1.1 – Variation on the Basic Wafer Preparation

In order to study the effects the iron catalyst had on the electrical conductivity across the aluminum oxide diffusion barrier, half of the wafers had iron deposited on the aluminum oxide just prior to spinning on the protective layer of photoresist. This was accomplished with our in-house thermal evaporator, JIM. The thickness of the iron thin film was monitored via crystal monitor, which reported 4 nm of iron had been deposited. Once the iron was deposited, the wafers were diced using the same process used to dice the other samples. For the sake of clarity, samples with iron will be referred to as iron samples, and samples without iron will be referred to as non-iron samples.

2.2 – Furnace Processing

Samples were subjected to one of three furnace treatments: the CNT growth process, a hydrogen anneal, or no furnace treatment. Samples that underwent the CNT growth process were placed in a Lindberg Blue M EW-33850 furnace. The furnace was purged with hydrogen and then brought up to 750 °C while flowing 311 SCCM of hydrogen. Once this temperature was achieved, 338 SCCM of ethylene gas was added to the system. After 50 minutes, argon was introduced into the system at 311 SCCM and the ethylene and hydrogen gases were shut off. The system was allowed to cool to 200 °C before samples were removed from the furnace.

Samples that were hydrogen annealed underwent a related but modified process. Samples were placed in the furnace and hydrogen was used to purge the system. The hydrogen flow was maintained at 311 SCCM while the furnace was heated to 750 °C. The furnace was left at 750 °C for 50 minutes before introducing argon at 311 SCCM into the system, shutting off the hydrogen, and allowing the system to cool to 200 °C before removing the samples.

Samples that had no furnace treatment never entered the furnace and served as control samples for the subsequent experiments. Both iron and non-iron samples were treated with all three of the furnace treatments explained above. A summary of the samples resulting from the wafer preparation and furnace processing can be found in table 1.

		Furnace Processes			
Samples	Iron Catalyst Present	CNT Growth Process	Hydrogen Anneal Process	No Furnace Process	Number of Samples SIMS Analyzed
Iron, CNT Growth	x	x			2
Iron, Annealed	x		x		1
Iron, No Furnace	x			x	2*
No Iron, CNT Growth		x			2
No Iron, Annealed			x		0
No Iron, No Furnace				x	1*

Table 1. A list of all the samples used in the experiments. The samples either did or did not have the iron catalyst. All the samples had one furnace process that was used to condition the samples. Listed in the final column is how many of each sample was sent for SIMS analysis. Numbers in this column with a * next to the number had one of those samples made into a carbon sample through carbon ion implantation. Samples in this column with more than one sample sent off for SIMS analysis, but without a * had one sample prepared as described in the previous section and one prepared with an additional plasma cleaning.

2.2.1 – CNT Removal

Iron samples that were processed with the CNT growth furnace treatment needed the resulting CNTs removed without affecting the underlying diffusion barrier of aluminum oxide. This was accomplished by rubbing these samples on a vel-cloth (Allied High Tech Inc.) which stripped the CNTs off the surface of the samples. SEM micrographs showed evidence of residual carbon left on the samples in some cases after this process, see figure 2. The effects of this residual

carbon on the subsequent experiments and how these effects were mitigated is detailed in the following sections.

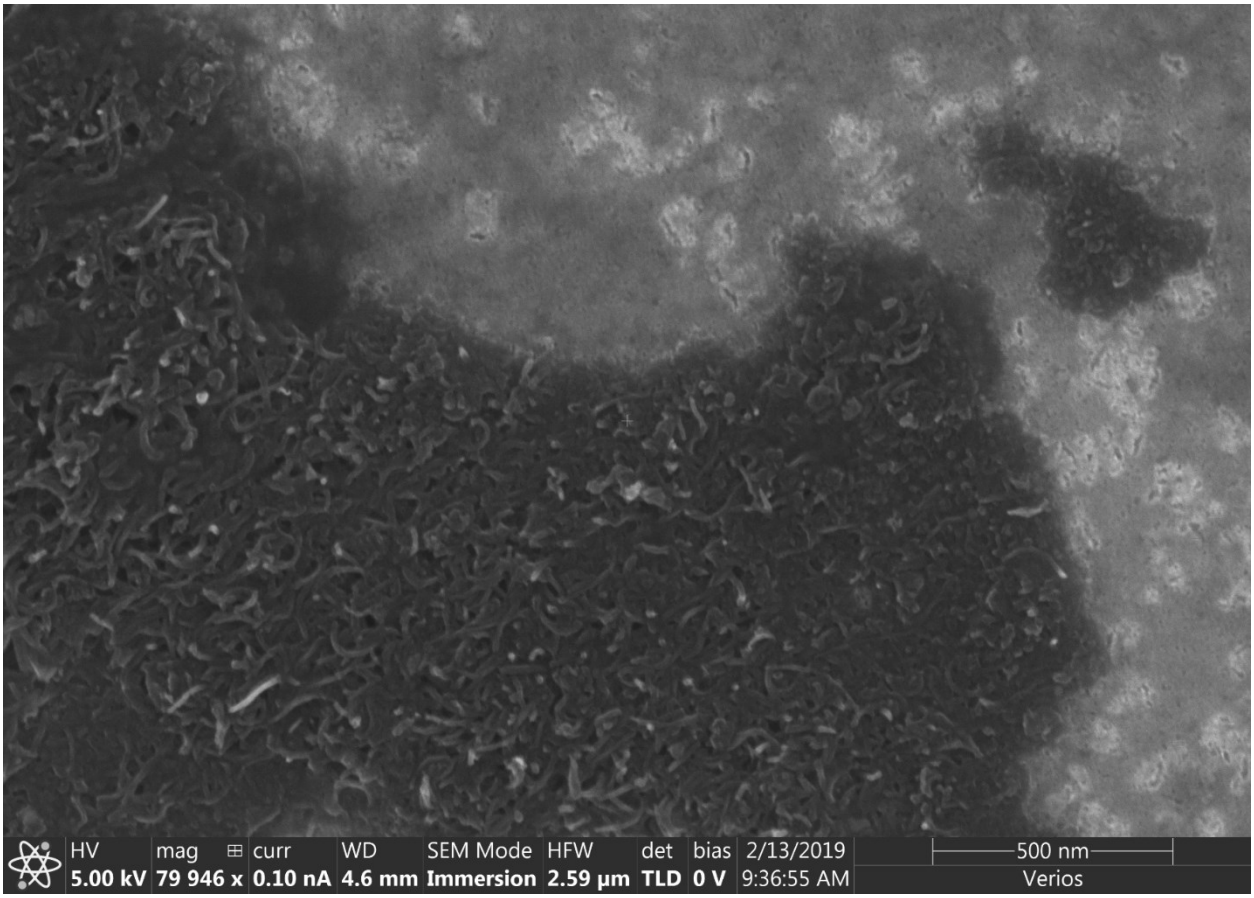

Figure 2. SEM micrograph of the surface of a carbon nanotube recipe processed iron sample after the nanotubes were removed with a vel-cloth. The surface of the aluminum oxide can be seen in the brighter, upper right side of the image while the residual carbon can be seen in the darker lower left side of the image.

2.3 – Electrical Measurements and Resistance Calculation

To determine average resistances through the diffusion barrier, electrical leads were attached to samples, and a series of I-V measurements were taken. Resistances for these measurements was calculated from the data collected during these measurements.

To attach electrical leads to the samples, 22-gauge copper magnet wire had its insulating enamel removed abrasively. 10 short pieces of this stripped wire were coated with MG Chemicals

8831-14G silver conductive epoxy. The epoxy-covered ends of the wire were secured to the samples in one of two general areas: four of the leads were attached to the exposed tungsten while the other six were attached to the aluminum oxide; for reference see figure 3. The samples were left to cure for a minimum of 10 hours before beginning the I-V measurements.

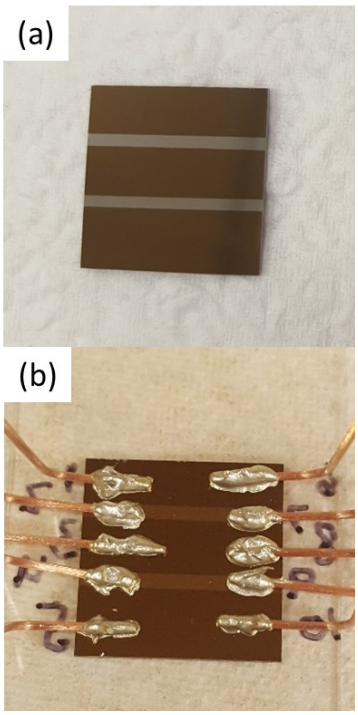

Figure 3. Image of a sample (a) before attaching the electrical leads and (b) after attaching the electrical leads to the tungsten and aluminum oxide. Running down each side of the sample, leads alternate between being tungsten and aluminum oxide leads. The brighter stripes running across the sample are the areas on the sample where the tungsten has been exposed and the darker regions are the diffusion barrier aluminum oxide. The resulting sample has four tungsten leads and six aluminum oxide leads.

For each sample, 20 I-V measurements were made between pairs of tungsten leads to determine if there was good electrical contact between the electrical leads and the sample. I-V measurements were also used to determine if current was able to cross the aluminum oxide diffusion barrier by making a minimum of 64 I-V measurement on each sample between a tungsten lead and an aluminum oxide lead. An additional minimum of 36 I-V measurements per sample were made between pairs of aluminum oxide leads to verify that there wasn't any electrical

shorting between aluminum oxide leads. Resistances for these measurements were calculated from an interpolated fit to the data collected from the I-V measurements. The MATLAB script used to calculate the samples' resistances, dataProcessor3.m, can be found in the appendix.

To assure that the resistance measured on the CNT growth treated samples was not influenced by graphitic carbon deposited on their surface during the CNT growth process, these samples were plasma cleaned. This was done with an expanded plasma cleaner (Harrick Plasma). The plasma cleaning was done while flowing atmosphere at 30 SCCM for 20 minutes on high power. Once the plasma clean was completed the I-V measurements for the CNT growth treated samples was collected.

2.3.1 – Modified Electrical Measurement Sample Preparation

In order to verify that surface carbon was not contributing to the drop of resistance that we were looking for, an additional set of CNT growth treated, iron and non-iron samples was prepared for I-V measurements using a modified preparation method. After exposing the samples to the CNT growth process and removing the CNTs with a vel-cloth in the case of the iron sample, instead of attaching electrical leads immediately to the samples, the plasma cleaning was performed before attaching the electrical leads to the samples. The difference between these samples and the samples described in the previous section is when the electrical leads were attached to the sample relative to when the plasma cleaning step was performed.

These samples were then measured using the same I-V measurements and resistance calculation used to characterize the other samples. By preparing and measuring these samples in this manner we were able to demonstrate that surface carbon was removed from our samples with the plasma cleaning. This conclusion is explained and expanded upon in section 3.1.1.

2.4 – Electron Microscopy Analysis

To collect STEM images of the aluminum oxide layer diffusion barrier, cross sections of the samples were made into TEM samples. This was accomplished by depositing a protective layer of gold-palladium alloy, 80 nm thick, on the samples using a Quorum Q1510T ES turbomolecular pumped coater. The samples were then put in an FEI Helios NanoLab 600 DualBeam FIB/SEM. An additional protective 5×20 μm^2 layer of platinum, 1 μm thick, was deposited on the sample prior to milling it out of the larger silicon die. This was accomplished by using the FIB to perform ion-beam-induced deposition with a (methylcyclopentadienyl)trimethyl platinum, $(CH_3)_3Pt(CpCH_3)$, precursor. A lamella was then made by removing the material around the area of interest with the FIB, welding the lamella to the microscope's omniprobe, removing the lamella from the sample, and finally welding the sample to a copper TEM sample holder and releasing the sample from the microscope's omniprobe. A 5 μm wide TEM window was made in the lamella by using the FIB to thin the sample, finishing the TEM sample preparation.

These TEM samples were put in an FEI Tecnai G^2 F20 TEM/STEM for observation and analysis. Using STEM, micrographs of the aluminum oxide layer in the samples were collected. XEDS was used to collect spectra to determine the chemical composition of the samples.

2.5 – Secondary Ion Mass Spectroscopy Analysis

In an attempt to obtain quantitative carbon content data about the samples, SIMS was used to analyze the samples. This involved making two carbon standard samples. A non-furnace processed iron sample and a non-furnace-processed non-iron sample were converted into these two carbon standards. To make these samples the carbon standards, they were sent to Leonard Kroko Inc. for carbon ion implantation, which was done at 10 keV and a dose of 10^{14} ions/cm^2.

Due to the cost of the SIMS analysis through AMPAC at UCF, only a subset of the samples used in the other experiments was selected for SIMS analysis. In addition to the carbon standards, the samples used for SIMS analysis included a non-furnace-processed, iron sample; a hydrogen annealed, iron sample; two CNT-growth furnace treated, iron samples, one was untreated beyond the processing listed through section 2.2.1 while the other had the plasma cleaning treatment described in section 2.3 in addition to processing the other sample received; two carbon processed non-iron samples, one was untreated beyond the processing listed through section 2.2.1 while the other had the plasma cleaning treatment outlined in section 2.3 in addition to processing the other sample received. For clarity, the information on samples that were SIMS analyzed is summarized in table 1. Prior to analysis, these samples were washed with deionized water and blown dry with nitrogen. SIMS analysis was performed using a PHI Adept 1010 Dynamic SIMS System using a cesium ion source. The data collect from these SIMS measurements was then analyzed with the following MATLAB scripts found in the appendix, SIMSBinning2.m, SIMSFieldnames.m, rebinning.m, and aluminumRatio.m.

Chapter 3 – Results and Discussion

3.1 – Data and Results

3.1.1 – Electrical Measurements

The resistances calculated from the I-V measurements can be found in table 2. Good electrical contact between the samples and the conductive epoxy coated leads is shown by the low average resistances between tungsten to tungsten contacts, see the first column of table 2.

Resistances for I-V measurements made between a tungsten and aluminum oxide lead varied based on which furnace process the sample had been subjected to. Samples that were hydrogen annealed exhibited resistances above 100 MΩ, which exceeds the maximum measureable resistance and was either greater than or comparable to the resistances attained by the same tungsten to aluminum oxide lead I-V measurement done on the non-furnace processed samples. A resistance of a few kiloohms was found when measuring between the tungsten and aluminum oxide leads on CNT growth processed iron samples, which is much lower than for the same measurement done on the non-furnace processed iron sample. CNT growth processed non-iron samples exhibited resistances near 20 Ω between tungsten and aluminum oxide leads, the lowest measured resistances except for measurements between tungsten to tungsten contacts. Samples that were exposed to the CNT growth recipe in the furnace had resistances decrease by roughly a factor of 10^3 to 10^7. This drop in resistance was present regardless of whether or not the samples had iron. While making this observation, the error bars on the aluminum oxide lead I-V measurements for the CNT growth processed iron sample should be discussed. The I-V measurements made for the tungsten to aluminum oxide leads and the pairs of aluminum oxide leads were bimodal, with measurements clumping either under 200 Ω or being over 6 kΩ.

Generally, the higher resistances were the result of a few specific aluminum oxide electrical leads that would produce high electrical measurements with all other lead pairings. However, in a few cases, these anomalous aluminum oxide leads would spontaneously exhibit resistances on the order of a couple hundred ohms and then resume their previous state exhibiting several thousand ohms. The resistances collected from these anomalous electrical leads are not being discarded on the grounds that we can find nothing wrong with them other than their erratic resistance behavior.

Recorded Resistances			
Samples	Resistance W to W leads (Ω)	Resistance W to Al_2O_3 leads (Ω)	Resistance Al_2O_3 to Al_2O_3 leads (Ω)
Iron, No Furnace	100 ± 116	1.5 E6 ± 6.25 E5	3.3 E6 ± 8.29 E5
No Iron, No Furnace	157 ± 41.1	> 1.0 E8	> 1.0 E8
Iron, Annealed	30 ± 21.2	> 1.0 E8	> 1.0 E8
No Iron, Annealed	19 ± 1.61	> 1.0 E8	> 1.0 E8
Iron, CNT Recipe	16 ± 1.3	3 E3 ± 5.62 E3	4 E3 ± 6.21 E3
No Iron, CNT Recipe	15.7 ± 0.901	18.0 ± 1.44	20 ± 1.17
Iron, CNT Recipe, Leads Attached After Plasma Clean	10.6 ± 0.704	> 1.0 E8	> 1.0 E8
No Iron, CNT Recipe, Leads Attached After Plasma Clean	19 ± 1.86	> 1.0 E8	> 1.0 E8

Table 2. Average resistances for each type of lead pairing measured for each of the samples.

The samples in the last two rows of table 2 are the samples that were prepared following the process described in section 2.3.1. These are the CNT growth processed samples where the

electrical leads were attached to the samples after they were plasma cleaned. The resistances calculated from the I-V measurements of these samples can be compared with the resistances for the conductive CNT growth processed samples whose electrical leads were attached prior to plasma cleaning. It is important to remember when making the comparison between these two groups of samples that the processing used to prepare them was identical except for when the electrical leads were attached to the samples. Looking at the resistances calculated for the I-V measurements between one tungsten lead and one aluminum oxide lead, it can be seen that these measurements are above the maximum resistance that could be measured with I-V probe station. This is unlike the samples where the leads where the leads where attached prior to plasma cleaning which are conductive. This suggests that whatever caused the samples to be conductive after the CNT growth processing has been reversed by the plasma cleaning if the electrical leads are not attached to the sample before the cleaning.

It can also be seen that the resistance between pairs of aluminum oxide leads in the samples where the electrical leads were attached after plasma cleaning them is above the maximum resistance that can be measured with our I-V probe station. This indicates that there are no conductive pathways between aluminum oxide leads in the case of these samples which suggests that any surface carbon deposited during the CNT growth recipe processing that could be shorting out pairs of aluminum oxide leads has been removed by the plasma cleaning. This conclusion can be extended to the samples where the electrical leads had been attached prior to the plasma cleaning which indicates that the conductive pathway between pairs of aluminum oxide leads in this case is down through the aluminum oxide, across the tungsten, and back up through the aluminum oxide instead of shorting out directly across the aluminum oxide.

3.1.2 – Electron Microscopy Data

TEM micrographs of the microstructure of the samples can be seen in figure 4. Figure 4.a shows the microstructure of the hydrogen annealed, non-iron sample. Figure 4.b-d shows the microstructure of the iron samples; specifically, they are the non-furnace processed sample, the hydrogen annealed sample, and CNT growth furnace treated sample, respectively. The dark thinner band at the top of these four micrographs is diffusion barrier aluminum oxide and the bright band immediately below the aluminum oxide is the conductive tungsten layer. The hydrogen annealed non-iron sample's aluminum oxide appears pristine: there are no inclusion in the aluminum oxide. The transition at the interfaces between the gold/palladium layer above the aluminum oxide and the tungsten layer below the aluminum oxide are immediate, too. All of the other non-iron samples had similar aluminum oxide layers as well. In the non-furnace processed, iron sample, in contrast to the non-iron sample, the transition from layer above the aluminum oxide to the aluminum oxide is not instantaneous, but occurs over a few nanometers going from bright to dark. This smeared transition is the iron deposited on the aluminum oxide. This transition can be seen better in the inset image in figure 4.b. In the hydrogen annealed and the CNT-growth furnace-treated iron samples, bright dots begin to appear within the aluminum oxide layer, see figure 4.c-d inset images. By using XEDS, it was determined that these dots were principally composed of iron. Figure 4.e shows the XEDS spectrum taken at the point indicated by the orange dot in figure 4.d for this verification. These little dots of iron within the aluminum oxide were evidence of iron diffusion in our furnace treated samples.

By performing an XEDS linescan across the aluminum oxide layers in the furnace processed iron samples, see figure 4.f taken across the orange line in the inset image in 4.d, it was possible to observe that the iron was concentrating inside the aluminum oxide layer. The highest

concentration of iron inside the aluminum oxide could be found in these bright dots of iron while a slightly elevated level of iron could be found at the surface of the aluminum oxide diffusion barrier.

It should be noted that the iron dots in CNT growth recipe processed iron sample, figure 4.d, are larger and penetrate further in the aluminum oxide than the iron dots in hydrogen annealed iron sample, figure 4.c. Iron that has diffused into the aluminum oxide layer in CNT growth processed iron samples is frequently seen in large nanoparticles as can be seen in figure 5. There have been iron nanoparticles in these samples that have been observed to have diameters as large as one third the depth of the aluminum oxide layer, and can penetrate most of the way through the aluminum oxide layer, as can be seen in figure 5, although none have been observed that have completely diffused across the aluminum oxide layer. In the hydrogen annealed iron samples, though, the nanoparticles that are observed are comparatively small compared to the larger nanoparticles in the CNT growth processed iron samples. These nanoparticles in the hydrogen annealed samples also remain close to the surface of the aluminum oxide, only penetrating a few nanometers, as is seen in the inset of figure 4.c.

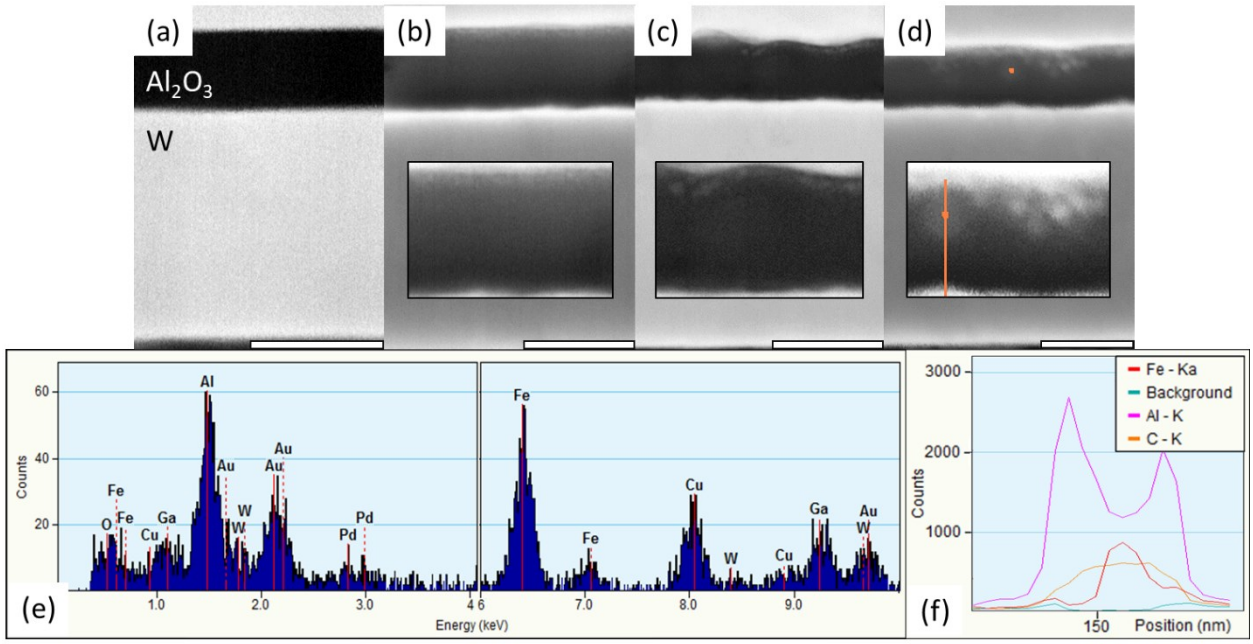

Figure 4. Electron micrographs (a-d) of several samples along with insets for the iron samples, and (e) two segments of the XEDS spectrum. The samples represented above are (a) the hydrogen annealed non-iron sample, (b) non-furnace processed iron sample, (c) hydrogen annealed iron sample, (d) CNT growth recipe processed iron sample. The orange dot in (d) indicates where the XEDS spectrum (e) was taken, while the orange line in the inset of image (d) indicates where the portion of the linescan in (f) was taken. Scale bars in (a-d) are 50 nm.

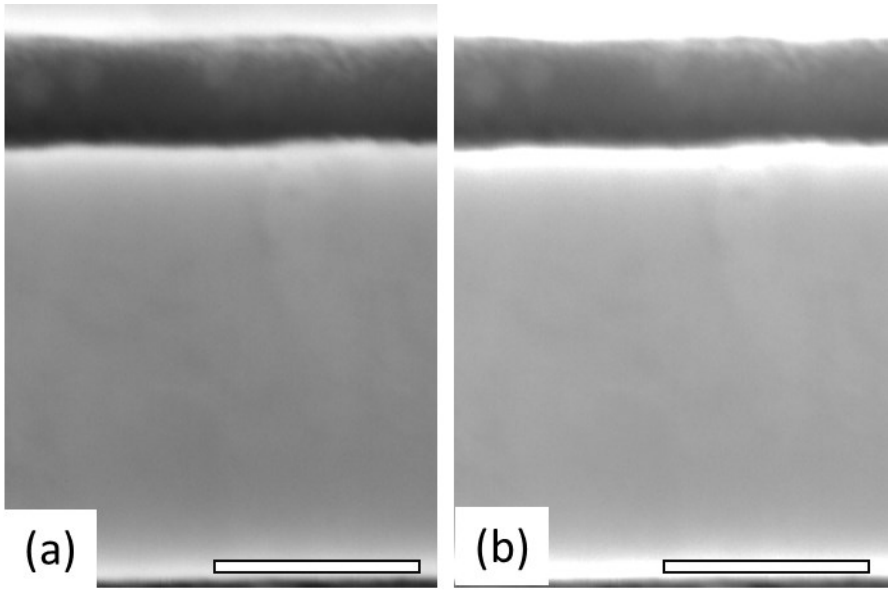

Figure 5. STEM images of a CNT growth processed, iron sample. Image (a) shows the original image taken and image (b) is the same image with modified brightness and contrast to highlight the diffused iron nanoparticles.

3.1.3 – Secondary Ion Mass Spectroscopy Data

SIMS profiles of two samples – a hydrogen annealed iron sample and a carbon ion implanted non-iron sample – can be seen in figure 6. The horizontal axis is representative of the sputter time and the vertical axis is the number of ion counts. Starting at the left of the profiles is the aluminum oxide diffusion barrier, deeper in the sample is the conductive tungsten layer and the subsurface layer of aluminum oxide. The aluminum oxide layers are marked by an increased level of aluminum ion counts while the tungsten layer is marked by an elevated level of the tungsten and carbon polyatomic ion counts. The transition between films in the material is marked by a spike in the ion counts. This transitional spike in counts between each layer is marked in figure 6 with black lines. In all the samples, including those not show in figure 6, there is a nontrivial amount of carbon counts throughout the surface aluminum oxide layer. This includes

samples that were exposed to carbon through the CNT growth furnace process or the carbon ion implantation as well as samples that didn't have any intentional carbon exposure – the hydrogen annealed sample and the non-furnace processed sample. This carbon content in the samples is so high that it masks the Gaussian distribution of carbon ions implanted in the carbon ion implanted samples, as seen in the top image in figure 6. This suggests that the background carbon in the samples is greater than the amount of carbon that was implanted in the ion implanted samples, making attempts at carbon quantification impossible.

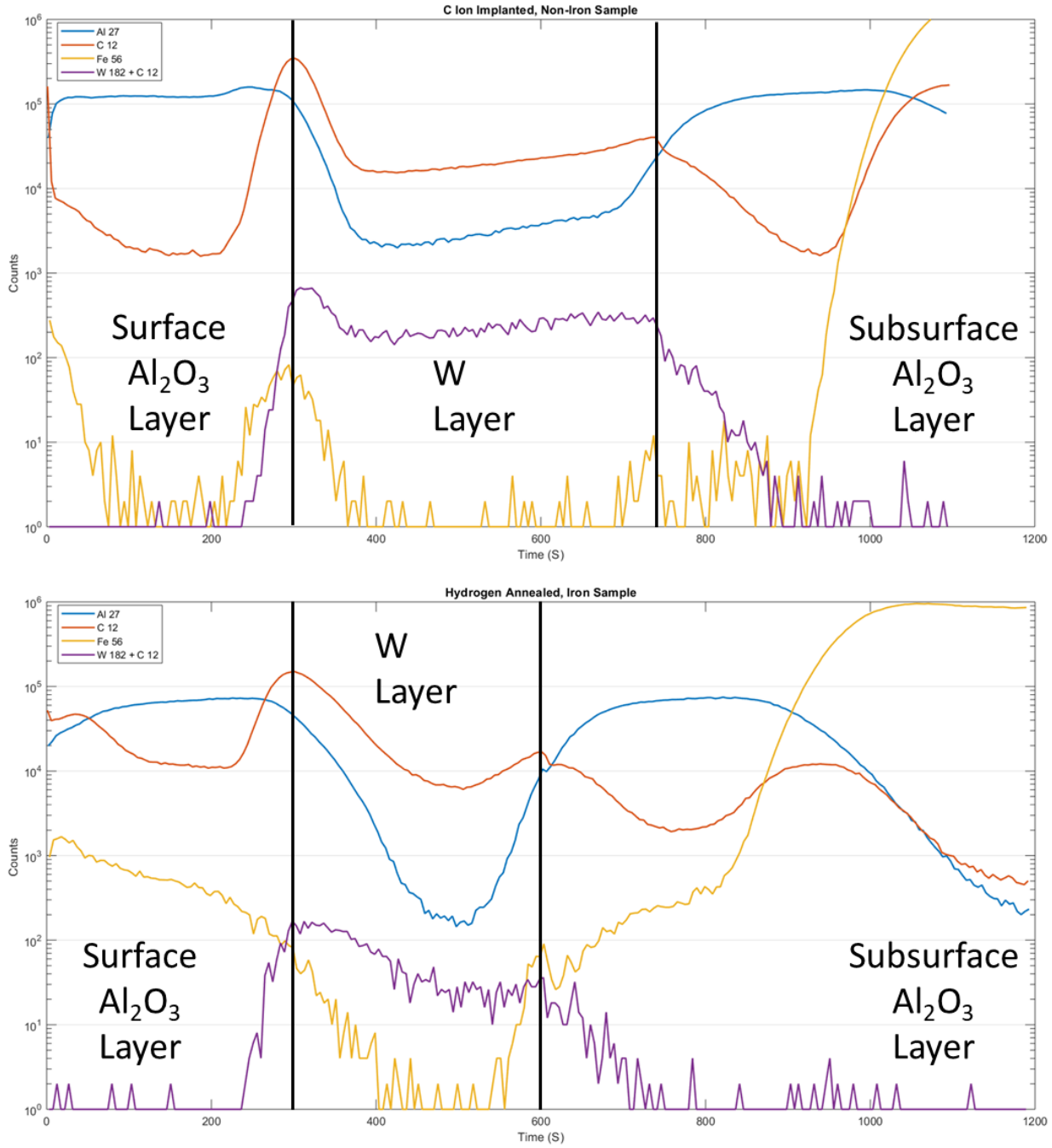

Figure 6. SIMS profiles of two samples that were analyzed. (Top) Carbon ion implanted non-iron sample depth profile. (Bottom) Hydrogen annealed iron sample. The region of interest in these samples is the surface aluminum oxide. This is the layer where the observed drop in resistance occurs during CNT growth recipe processing. In all the samples, including the two given here, a nontrivial amount of carbon ion counts are collected in the surface and subsurface aluminum oxide layers.

Despite these unexpected results, there is a reliable level of repeatability in the profiles taken as can be seen in figure 7. This figure shows two separate runs that were done on the CNT growth recipe processed iron samples that was only polish cleaned prior to analysis. This level of consistency was found in all of the samples where repeat runs where performed, suggesting a reliable level of repeatability.

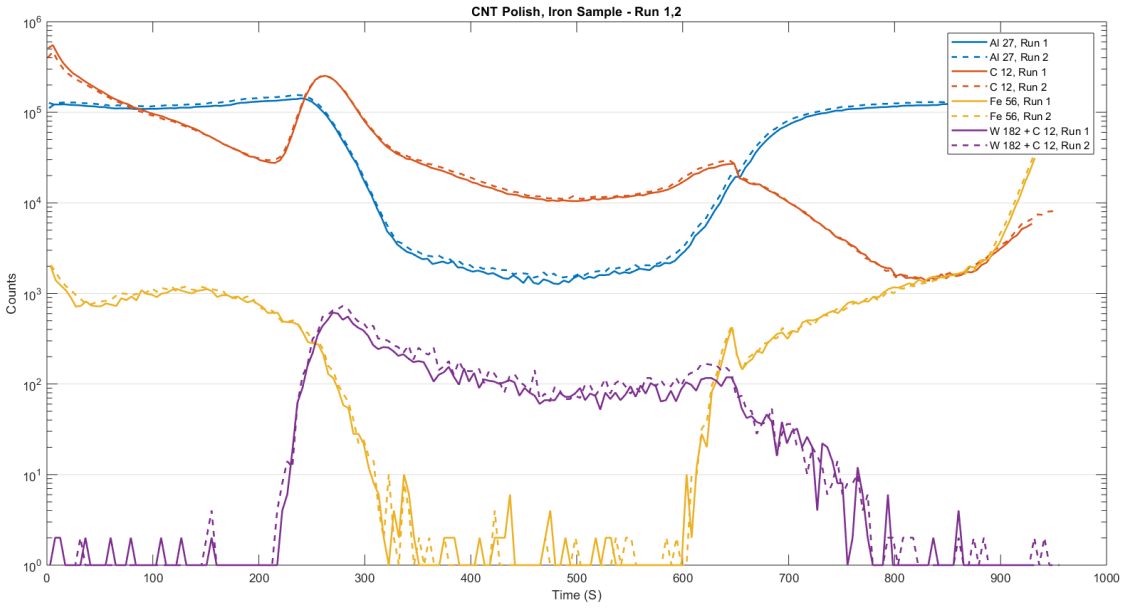

Figure 7. Sputtering data from two depth profiles that were done on the same CNT polish, iron sample.

An attempt to compare the carbon content in the aluminum oxide diffusion barrier across all the samples was done by normalizing the carbon ion counts by the aluminum ion counts. The resulting data can be seen in figure 8.

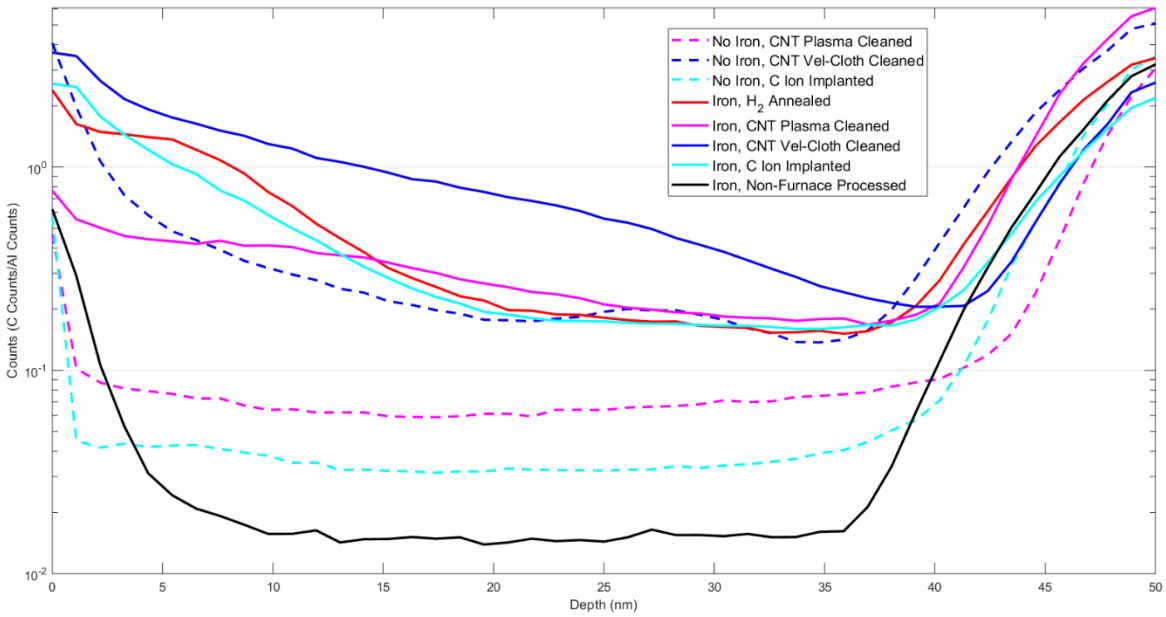

Figure 8. Depth profile of the ratio of the carbon counts to the aluminum counts in the surface aluminum oxide layer. This ratio aids in making a comparison of carbon content in each sample with the other samples. The trend of counts rising toward the end is the result of aluminum counts dropping off before the carbon counts.

In figure 8, there are some artifacts that need to be recognized before making any conclusions. The first artifact is that all the samples' carbon-to-aluminum ratio counts start to increase towards the bottom of the diffusion barrier. This is a result of the interface effects; the carbon counts spike and the aluminum counts drop off as the sputtering transitioned to the tungsten layer, making it difficult to make any conclusions based on the data from the last 10 nm in this depth profile. The second is how some of the counts drop off rapidly during the first 5 nm of the depth profile before stabilizing. This can occur for a variety of reasons including higher carbon levels on the surface of some samples. However, when we look at the region of figure 8 between 5 and 40 nm where the curves are more stable, it is difficult to draw any correlations between any processing parameters and the carbon content of a sample. Samples that were CNT growth furnace processed or carbon ion implanted and exposed to carbon seem to cluster together in figure 8.

Within this cluster, though, is the hydrogen annealed sample which was not exposed carbon. There are also two samples that were exposed to carbon – the carbon ion implanted, non-iron sample and the plasma cleaned, CNT growth furnace processed, non-iron sample – that are closer to the non-furnace processed sample, which was not exposed to carbon, than to the other carbon exposed samples.

3.2 – Discussion

The data collected draws us towards a couple of conclusions about the electrical conductivity across the aluminum oxide in our specific case. The first is that catalyst diffusion into the aluminum oxide layer did not contribute to the drop in resistance. We observed iron diffusion in all of the samples that had the catalyst and were furnace processed, both the annealed and carbon processed samples, but only the samples that went through the CNT growth furnace recipe show any decrease in the resistance across the aluminum oxide diffusion barrier. From the STEM images and XEDS spectra collected, it does not seem that the iron significantly dopes the aluminum oxide as it diffuses into it but rather collects in isolated pockets within the aluminum oxide. Additionally, these iron pockets are observed in a higher concentration towards the surface of the aluminum oxide diffusion barrier and there is a decrease in the number of these iron pockets the closer you get to the tungsten layer.

The second conclusion from the data is that running the full carbon nanotube recipe, heating the sample while flowing both hydrogen and critically ethylene, is essential to making conductive pathways across the aluminum oxide diffusion barrier. It was only in samples where this occurred, both with and without iron, that a significant decrease in the resistance across the aluminum oxide layer was observed. However, the possible simple picture of carbon diffusion into, and thus doping, the aluminum oxide diffusion barrier is insufficient. From the SIMS depth

profiles, we see that there is significant number of carbon counts present in all the samples, both those that show low electrical resistivity and those that are highly resistive. Thus, it would appear that the manner in which the sample is exposed to carbon is more significant than the overall carbon content of the sample.

Several models of how exposure to carbon via ethylene gas in the furnace induces low conductivity across the aluminum oxide diffusion barrier have been explored. A simple model, as mentioned above, is diffusional doping of the aluminum oxide diffusion barrier with carbon. The presence of carbon in all of the samples, including the samples that have not seen any furnace processing and those that were hydrogen annealed, implies that carbon is being incorporated in the e-beam deposited aluminum oxide during deposition. Thus, the presence of carbon in the film is not able to explain the different conductivities.

A second possible model is that carbon reduces the aluminum oxide, i.e. carbothermic reduction of the aluminum oxide. While a reduction of the aluminum oxide to a more conductive aluminum carbide or even aluminum could account for the change in conductivity, the literature seems to indicate that the temperature required to initiate any reaction between the aluminum oxide and carbon would be at least 1500 °C with pure aluminum beginning to appear at temperatures around 2100 °C [56,57]. This would preclude the reaction from occurring in our 750 °C furnace.

A third possibility is that there are pinholes in the aluminum oxide that are being filled with conductive carbon deposited on the surface by CNT growth process. It is known that electron beam evaporated aluminum oxide is porous [39,58]. We suggest that these pinholes are being filled with pyrolytic carbon and shorting across the aluminum oxide. Support for this model can be seen in the electrical measurements. Samples that had their aluminum oxide leads attached after the plasma cleaning demonstrate resistances as large as if not larger than their respective control

samples while the samples that had their leads attached prior to the plasma cleaning are conductive. This implies the plasma cleaning is capable of reversing whatever changes happened during the carbon processing, but if the surface of the sample is shielded from the reactive atmospheric plasma, by the attached electrical leads, this reversal does not occur. Since this plasma removes the surface carbon and the surface carbon would be shielded by the attached leads, we suggest this to be a possible explanation of what is happening.

Chapter 4 – Conclusion and Future Work

4.1 – Conclusion

Electrically insulating aluminum oxide diffusion barriers used for CNT forest growth become conductive after CNT growth. Experiments were carried out to probe the mechanism responsible for this transformation. Samples were fabricated with a conductive tungsten layer covered with an aluminum oxide diffusion barrier. Samples with and without the iron catalyst were subjected to portions of the CNT growth process and then characterized by I-V measurements, electron microscopy, and SIMS analysis. Data from these experiments indicate that a heat treatment at 750 °C while flowing both hydrogen and ethylene was necessary to cause this change in the samples. Samples were not conductive prior to being placed in the furnace nor after hydrogen annealing the samples without ethylene. XEDS and STEM imaging show evidence of iron diffusion in samples that were heated to 750 °C, but this condition was not correlated to a change in aluminum oxide resistance, as is suggested in the literature. The presence of carbon in the aluminum oxide layer was also not conclusively indicative of a change in conductivity since all samples analyzed by SIMS in this study had a detectable carbon content in the aluminum oxide diffusion barrier, but not all of these samples were conductive. We suggest that since the presence of ethylene during furnace processing was essential for this change in conductivity there is a link between carbon deposition during furnace processing that while not significantly altering the overall carbon content of the sample is responsible for this change, potentially carbon collecting at grain boundaries or pinholes being filled with carbon.

4.2 – Future Work

A carbon filled pinholes model has several implications that can be tested for further verification of this model. First, pinhole density would be expected to impact the final film

conductivity. By using several aluminum oxide deposition methods, it would be possible to alter the pinhole density in the sample. By using several deposition methods, such as ALD or sputtering instead of electron beam evaporation, to deposit the aluminum oxide and control the films porosity it should be possible to influence how much the resistance across the aluminum oxide changes, or even prevent the change from happening.

Conductive carbon filled pinholes could also be found by using a direct observation. By using EBIC or conductive AFM (C-AFM) it should be possible to image the conductive areas on the CNT growth processed samples. If there are conductive pinholes or grain boundaries, we expect them to be in discrete locations across the sample and that they would show up as an area of different contrast. However, if the samples are being doped, we would expect the doping to be isotropic across the surface of the aluminum oxide. This would result in an image that is fairly uniform and doesn't have any areas of high contrast. By utilizing EBIC or C-AFM it will be possible to find direct evidence for whether carbon doping or carbon collecting at grain boundaries or packing pinholes is the mechanism causing the drop in resistance.

As this study only used one thickness for the aluminum oxide and one growth time, it could be instructive to vary the aluminum oxide diffusion barrier thicknesses and growth times to see how these parameters affect the change in resistance across the aluminum oxide. A thinner aluminum oxide layer would allow greater carbon penetration through shorter pinholes and could allow the iron catalyst to play a more significant role in conductivity, thicker aluminum oxide could show limits to filled pinholes reaching through the layer. Varying growth times could indicate how much carbon deposition is needed to create these conductive pathways.

References

1. Hutchison, D. N. *et al.* Carbon Nanotubes as a Framework for High-Aspect-Ratio MEMS Fabrication. *J. Microelectromechanical Syst.* **19**, 75–82 (2010).
2. Ruoff, R. S., Qian, D. & Liu, W. K. Mechanical properties of carbon nanotubes: theoretical predictions and experimental measurements. *Comptes Rendus Phys.* **4**, 993–1008 (2003).
3. Gao, G., Çagin, T. & Goddard, W. A. Energetics, structure, mechanical and vibrational properties of single-walled carbon nanotubes. *Nanotechnology* **9**, 184–191 (1998).
4. Roche, S. Carbon nanotubes: Exceptional mechanical and electronic properties. *Ann. Chim. Sci. Matér.* **25**, 529–532 (2000).
5. Wilder, J. W. G., Venema, L. C., Rinzler, A. G., Smalley, R. E. & Dekker, C. Electronic structure of atomically resolved carbon nanotubes. *Nature* **391**, 59–62 (1998).
6. Bandaru, P. R. Electrical Properties and Applications of Carbon Nanotube Structures. *J. Nanosci. Nanotechnol.* **7**, 1239–1267 (2007).
7. Hone, J. *et al.* Thermal properties of carbon nanotubes and nanotube-based materials. *Appl. Phys. A* **74**, 339–343 (2002).
8. Ruoff, R. S. & Lorents, D. C. Mechanical and thermal properties of carbon nanotubes. *Carbon* **33**, 925–930 (1995).
9. Zhong, G. *et al.* Growth of Ultrahigh Density Single-Walled Carbon Nanotube Forests by Improved Catalyst Design. *ACS Nano* **6**, 2893–2903 (2012).
10. Toone, N. C. *et al.* Investigation of Unique Carbon Nanotube Cell Restraint Compliant Mechanisms. *Mech. Based Des. Struct. Mach.* **42**, 343–354 (2014).

11. Hanna, B. H. *et al.* Mechanical Property Measurement of Carbon Infiltrated Carbon Nanotube Structures for Compliant Micromechanisms. *J. Microelectromechanical Syst.* **23**, 1330–1339 (2014).
12. Pitkänen, O. *et al.* On-chip integrated vertically aligned carbon nanotube based super- and pseudocapacitors. *Sci. Rep.* **7**, 16594 (2017).
13. Sugano, K. *et al.* Fabrication and characterization of a CNT forest integrated micromechanical resonator for a rarefied gas analyzer in a medium vacuum atmosphere. *J. Micromechanics Microengineering* **26**, 075010 (2016).
14. Zang, X., Zhou, Q., Chang, J., Liu, Y. & Lin, L. Graphene and carbon nanotube (CNT) in MEMS/NEMS applications. *Microelectron. Eng.* **132**, 192–206 (2015).
15. Chen, G. *et al.* Tissue-susceptibility matched carbon nanotube electrodes for magnetic resonance imaging. *J. Magn. Reson.* **295**, 72–79 (2018).
16. Bareket-Keren, L. & Hanein, Y. Carbon nanotube-based multi electrode arrays for neuronal interfacing: progress and prospects. *Front. Neural Circuits* **6**, (2013).
17. David-Pur, M., Bareket-Keren, L., Beit-Yaakov, G., Raz-Prag, D. & Hanein, Y. All-carbon-nanotube flexible multi-electrode array for neuronal recording and stimulation. *Biomed. Microdevices* **16**, 43–53 (2014).
18. Barrett, L. K. *et al.* High-Aspect-Ratio Metal Microfabrication by Nickel Electroplating of Patterned Carbon Nanotube Forests. *J. Microelectromechanical Syst.* **24**, 1331–1337 (2015).
19. Jordan, M. B., Feng, Y. & Burkett, S. L. Development of seed layer for electrodeposition of copper on carbon nanotube bundles. *J. Vac. Sci. Technol. B* **33**, 021202 (2015).
20. Akhtar, M. S., An, Z., Toda, M. & Ono, T. Electrodeposition and characterization of nickel-carbon nanotube composite thin films with high carbon nanotube content. in *2016 IEEE 16th*

International Conference on Nanotechnology (IEEE-NANO) 904–906 (2016). doi:10.1109/NANO.2016.7751464.

21. Kanyal, S. *et al.* Atomic layer deposition of aluminum-free silica onto patterned carbon nanotube forests in the preparation of microfabricated thin-layer chromatography plates. *JPC - J. Planar Chromatogr. - Mod. TLC* **27**, 151–156 (2014).
22. Song, J. *et al.* Carbon-Nanotube-Templated Microfabrication of Porous Silicon-Carbon Materials with Application to Chemical Separations. *Adv. Funct. Mater.* **21**, 1132–1139 (2011).
23. Jensen, D. S. *et al.* Ozone priming of patterned carbon nanotube forests for subsequent atomic layer deposition-like deposition of SiO2 for the preparation of microfabricated thin layer chromatography plates. *J. Vac. Sci. Technol. B* **31**, 031803 (2013).
24. Jensen, D. S. *et al.* Stable, microfabricated thin layer chromatography plates without volume distortion on patterned, carbon and Al2O3-primed carbon nanotube forests. *J. Chromatogr. A* **1257**, 195–203 (2012).
25. Delhaes, P. Chemical vapor deposition and infiltration processes of carbon materials. *Carbon* **40**, 641–657 (2002).
26. Gu, Z. *et al.* Aligned carbon nanotube-reinforced silicon carbide composites produced by chemical vapor infiltration. *Carbon* **49**, 2475–2482 (2011).
27. Kilpatrick, S. J., Anyuan Cao, Xuesong Li, Renna, N. J. & Ajayan, P. M. Densified Vertically-Aligned Carbon Nanotube Arrays by Chemical Vapor Infiltration. in *2005 International Semiconductor Device Research Symposium* 352–353 (2005). doi:10.1109/ISDRS.2005.1596131.

28. Lee, J. *et al.* High-strength carbon nanotube/carbon composite fibers via chemical vapor infiltration. *Nanoscale* **8**, 18972–18979 (2016).
29. Rümmeli, M. H. *et al.* Synthesis of carbon nanotubes with and without catalyst particles. *Nanoscale Res. Lett.* **6**, 303 (2011).
30. Jourdain, V. & Bichara, C. Current understanding of the growth of carbon nanotubes in catalytic chemical vapour deposition. *Carbon* **58**, 2–39 (2013).
31. Jodin, L., Dupuis, A.-C., Rouvière, E. & Reiss, P. Influence of the Catalyst Type on the Growth of Carbon Nanotubes via Methane Chemical Vapor Deposition. *J. Phys. Chem. B* **110**, 7328–7333 (2006).
32. Wei, Y. Y., Eres, G., Merkulov, V. I. & Lowndes, D. H. Effect of catalyst film thickness on carbon nanotube growth by selective area chemical vapor deposition. *Appl. Phys. Lett.* **78**, 1394–1396 (2001).
33. Suriani, A. B. *et al.* Effect of Iron and Cobalt Catalysts on The Growth of Carbon Nanotubes from Palm Oil Precursor. *IOP Conf. Ser. Mater. Sci. Eng.* **46**, 012014 (2013).
34. Homma, Y. *et al.* Role of Transition Metal Catalysts in Single-Walled Carbon Nanotube Growth in Chemical Vapor Deposition. *J. Phys. Chem. B* **107**, 12161–12164 (2003).
35. Zhao, N. & Kang, J. Direct Growth of Carbon Nanotubes on Metal Supports by Chemical Vapor Deposition. *Carbon Nanotub. - Synth. Charact. Appl.* (2011) doi:10.5772/19275.
36. Sohn, J. I., Choi, C.-J., Lee, S. & Seong, T.-Y. Growth behavior of carbon nanotubes on Fe-deposited (001) Si substrates. *Appl. Phys. Lett.* **78**, 3130–3132 (2001).
37. de los Arcos, T. *et al.* Influence of iron–silicon interaction on the growth of carbon nanotubes produced by chemical vapor deposition. *Appl. Phys. Lett.* **80**, 2383–2385 (2002).

38. Lee, H. C. *et al.* Multi-barrier layer-mediated growth of carbon nanotubes. *Thin Solid Films* **516**, 3646–3650 (2008).

39. Amama, P. B. *et al.* Influence of Alumina Type on the Evolution and Activity of Alumina-Supported Fe Catalysts in Single-Walled Carbon Nanotube Carpet Growth. *ACS Nano* **4**, 895–904 (2010).

40. Mattevi, C. *et al.* In-situ X-ray Photoelectron Spectroscopy Study of Catalyst−Support Interactions and Growth of Carbon Nanotube Forests. *J. Phys. Chem. C* **112**, 12207–12213 (2008).

41. de los Arcos, T. *et al.* Strong influence of buffer layer type on carbon nanotube characteristics. *Carbon* **42**, 187–190 (2004).

42. de los Arcos, T. *et al.* The Influence of Catalyst Chemical State and Morphology on Carbon Nanotube Growth. *J. Phys. Chem. B* **108**, 7728–7734 (2004).

43. *CRC materials science and engineering handbook*. (CRC Press, 2001).

44. Chen, G., Shin, D. H., Iwasaki, T., Kawarada, H. & Lee, C. J. Enhanced field emission properties of vertically aligned double-walled carbon nanotube arrays. *Nanotechnology* **19**, 415703 (2008).

45. Simmons, J. M. *et al.* Critical Oxide Thickness for Efficient Single-Walled Carbon Nanotube Growth on Silicon Using Thin SiO2 Diffusion Barriers. *Small* **2**, 902–909 (2006).

46. Sridhar, S. *et al.* Enhanced Field Emission Properties from CNT Arrays Synthesized on Inconel Superalloy. *ACS Appl. Mater. Interfaces* **6**, 1986–1991 (2014).

47. Ahmad, M. *et al.* High Quality Carbon Nanotubes on Conductive Substrates Grown at Low Temperatures. *Adv. Funct. Mater.* **25**, 4419–4429 (2015).

48. Sepahvand, S., Safaei, P. & Sanaee, Z. Growth of Carbon Nano Tubes on Copper Substrate Suitable for Lithium Ion Battery Anode. *Procedia Mater. Sci.* **11**, 634–638 (2015).
49. Kimura, H. *et al.* Field emission from laterally aligned carbon nanotube flower arrays for low turn-on field emission. *APL Mater.* **1**, 032101 (2013).
50. Chen, G. *et al.* Low turn-on and uniform field emission from structurally engineered carbon nanotube arrays through growth on metal wire mesh substrates. *Mater. Res. Express* **4**, 105041 (2017).
51. Hiraoka, T. *et al.* Synthesis of Single- and Double-Walled Carbon Nanotube Forests on Conducting Metal Foils. *J. Am. Chem. Soc.* **128**, 13338–13339 (2006).
52. Chen, G. *et al.* Fabrication of High Aspect Ratio Millimeter-Tall Free-Standing Carbon Nanotube-Based Microelectrode Arrays. *ACS Biomater. Sci. Eng.* **4**, 1900–1907 (2018).
53. Azam, M. A., Isomura, K., Ismail, S., Mohamad, N. & Shimoda, T. Electrically conductive aluminum oxide thin film used as cobalt catalyst-support layer in vertically aligned carbon nanotube growth. *Adv. Nat. Sci. Nanosci. Nanotechnol.* **6**, 045008 (2015).
54. Parthangal, P. M., Cavicchi, R. E. & Zachariah, M. R. A generic process of growing aligned carbon nanotube arrays on metals and metal alloys. *Nanotechnology* **18**, 185605 (2007).
55. Kim, S. M. *et al.* Evolution in Catalyst Morphology Leads to Carbon Nanotube Growth Termination. *J. Phys. Chem. Lett.* **1**, 918–922 (2010).
56. Halmann, M., Epstein, M. & Steinfeld, A. Carbothermic Reduction of Alumina by Natural Gas to Aluminum and Syngas: A Thermodynamic Study. *Miner. Process. Extr. Metall. Rev.* **33**, 352–361 (2012).
57. Halmann, M., Frei, A. & Steinfeld, A. Carbothermal reduction of alumina: Thermochemical equilibrium calculations and experimental investigation. *Energy* **32**, 2420–2427 (2007).

58. He, L., Li, C. & Liu, X. The optical properties of alumina films prepared by electron beam evaporation at oblique incidence. *Mater. Lett.* **101**, 1–4 (2013).

Appendix

dataProcessor3.m:

```
%Program: dataProcessor3.m
%Author: Berg Dodson
%Version: 3.1.1-finished
%Dependent Files: N/A
%Input: .csv files
%Output: Figures of the V vs I plots and .txt files containing a calculated
%   resistance
%Description: Analyzes the data that has been taken on the four point probe
%station and makes the plots of the measurements similar to those on the
%labview program running the station. The difference is that the curves
%are interpolated from the data recorded by the LabVIEW. The program
%also returns a resistance for the measurement by calculating the slope of
%of the interpolated IV curve.


clear; close all;

%import the files
dir = dir('*.csv');
numfiles = length(dir);

% To be used if you only want to analyze specific measurements from the
% files, uncomment the if statement below to use this feature.
keepers = [17,16,15,14,13,12,11,10,7,6,5,2,1];

for a= 1:numfiles
   if ~isempty(1)%find(keepers==a,1)) %replace when you know what the
       %keepers are

    %pulling out all of the data
    filename = dir(a).name;
    file = importdata(filename);
    filevolts = file(1,1:end);
    filecurrent = file(2,1:end);

    %getting the resistance
    %Setting the interpolated voltage
    minvolts = min(filevolts);
    maxvolts = max(filevolts);
    dv = maxvolts/(numel(filevolts)-1);
    vinterp = minvolts:dv:maxvolts;

    %Getting grid for interpolation
    maxvoltsI = find(filevolts == maxvolts);
    vsample = filevolts(maxvoltsI:end);
    isample = filecurrent(maxvoltsI:end);

    %Sorting current and voltage to be interpolated
    %Note: the difference between sort() and sortrows() is that sort will
    %sort all the columns of your matrix, while sortrows will sort
    %according to one column and move all the data in a given row as a
    %group. There are ways of specifying which row to sort by. See the
```

```
    %documentation.
    sorter = [vsample;isample].';
    sorted = sortrows(sorter).';
    sortedvolts = sorted(1,:);
    sortedcurrent = sorted(2,:);
    vinterp = sortedvolts;

    %getting the interpolated current
    %Note: the X and F(X) vectors that are input to create Finterp(Xinterp)
    %must contain unique points. In other words Vinterp cannot have
    %duplicate points. B/C of this, I will be using points on the downward
    %sweep, ie. sweep from highest to lowest voltage, since that has
    %yielded the data with the least amount of noise (Generally)


    [cinterpcoef,S] = polyfit(sortedvolts,sortedcurrent,1);
    cinterp = polyval(cinterpcoef,vinterp);

    %Plotting the new interpolation
    %Note: the saveas function saves the parent figure. If something else
    %aside from the parent figure is passed to the saveas function, it will
    %attempt to save the parent figure. However, there are some things that
    %the function does not like, so it is safest to always pass a figure
    %object to the saveas function after populating it with the things you
    %need.

    tosave = figure;
    plot(vinterp,cinterp,'r-',sortedvolts,sortedcurrent,'bo',filevolts,...
        filecurrent,'gx');
    title('Resistance Measurements')
    xlabel('Voltage (V)')
    ylabel('Current (A)')

    %Calculating the interpolated resistance from a finite difference V=IR
    %=> R = V/I
    Resistance = (vinterp(end)-vinterp(end-1))/...
        (cinterp(end)-cinterp(end-1));

    %Saving the plot
    savename = strcat(filename(1:end-3),'tif');
    saveas(tosave,savename);

    %saving the resistance
    savename = strcat(savename(1:end-3),'txt');
    resist = fopen(savename,'w');
    fprintf(resist,'%.3E',Resistance);
    fclose(resist);

   end
end

close all; clear;
```

SIMSBinning2.m:

```
%Title: SIMSBinning2.m
%Author: Berg Dodson
%Date: 9.Aug.2019
%Version: 2
%Dependent Files: SIMSFieldnames.m, rebinning.m, aluminumRatio.m
%Description: 1) Imports the trace data of two elements from each SIMS
%measurement. One of the traces is of the element of interest (EoI), the
%other is a of a standard element (SE) to normalize the EoI to. 2) The
%traces are then rebinned according to the shortest alumina data trace so
%they can be plotted with respect to depth. Once that is done, 3) the ratio
%of EoI/SE is taken and put into a new array 4) which is plotted and saved


%Selecting the files to analyze
clear; close all;

%EoI Files
EoIDirFiles = '*-*.xlsx';
EoIsimsFiles = dir(char(EoIDirFiles));
numFiles = numel(EoIsimsFiles);

%Standard Files
StandardFilepath = fullfile('..','..','Individual Sample Al Scans',...
    'Cs Source');
StandardFiles = EoIDirFiles;
StandardDir = dir(char(StandardFiles));

%Debug test
if numel(StandardDir) ~= numFiles
     '# Al files not match # C files'
end

%Struct to link the file name to the data in that file
EoIScans = struct;
StandardScans = struct;

%For loop to determine the shortest data file
shortestFile = 0;
fileLength = 0;

%loop does: 1) imports data from each file 2) creates a key to access that
%data later 3) stores data with key access in struct 4)determine the
%binning size for data to be used later
for a = 1:numFiles
    EoIFilename = EoIsimsFiles(a).name;
    standardFilename = fullfile(StandardFilepath, EoIFilename);

    EoIdata = importdata(EoIFilename);
    standardData = importdata(standardFilename);

    %aquire keys for the strut
    EoIkey = SIMSFieldnames(EoIFilename);
    StandardKey = SIMSFieldnames(standardFilename);
```

```
    %Save all of the data from each file to matlab var. 1 column is depth,
    %second column is counts
    EoIScans.(EoIkey) = EoIdata.data;
    StandardScans.(StandardKey) = standardData.data;

    %debug test
        if StandardKey ~= EoIkey
            'keys do not match'
            EoIkey
            StandardKey
            return
        end

    %Initialize file length counter and update it as necessary/(4)
    %determine binning size/file to determine binning size
    if fileLength == 0
        fileLength = length(EoIdata.data);
        shortestFile = EoIkey;
    elseif fileLength > length(EoIdata.data)
        fileLength = length(EoIdata.data);
        shortestFile = EoIkey;
    end

end

% variables for reformatting
binStep = 50/(fileLength - 1); %50nm/(Samples - 1)
keys = fieldnames(EoIScans);
ratioList = struct;

%rebinning all the data
for a = 1:length(keys)
%     keys{a}
    if ~strcmp(keys{a},shortestFile)
        EoIScans.(keys{a}) = rebinning(EoIScans.(keys{a}), binStep);
        StandardScans.(keys{a}) = ...
            rebinning(StandardScans.(keys{a}),binStep);
    end

    %creating the ratio list
%     keys{a}
    ratioList.(keys{a}) = aluminumRatio(EoIScans.(keys{a}), ...
        StandardScans.(keys{a}));
end

%Styles to rotate through in the plots
colors = {'r','k','b','g'};
styles = {'-','-.','o','x','s','d'};
legendEntries = {'Non-Fe Sample, Carbon Processed',...
    'Non-Fe Sample, Carbon Processed', 'Non-Fe Sample, Ion Implanted',...
    'Fe Sample, H_2 Annealed', 'Fe Sample, Carbon Processed',...
    'Fe Sample, Carbon Processed', 'Fe Sample, Ion Implanted',...
    'Fe Sample, No Furnace Treatment'};

%plotting the data overlay of all traces
tosave = figure('WindowState', 'maximized');
```

```
ax = gca;
for a = 0:length(keys)-1
    style = strcat(colors{mod(a,numel(colors))+1},...
        styles{floor(a/numel(colors)+1)});
    p = semilogy(ratioList.(keys{a+1})(:,1),...
        ratioList.(keys{a+1})(:,2),style);
    p.LineWidth = 2;
    hold on
end
title('Carbon/Al ratio')
xlabel('Depth (nm)')
ylabel('Counts (C Counts/Al Counts)')
legend(keys)%legendEntries)
ax.YLim =[10E-3 inf];
ax.YGrid = 'on';
ax.YMinorGrid = 'off';
hold off

%Saving overlay plot
savename = 'Figure Test3.tif';

saveas(tosave,savename);


clear; close all;
```

SIMSFieldnames.m:

```
%Title: SIMSFieldnames.m
%Author: Berg Dodson
%Version: 2 (Version 1 commented out at top of function)
%Date: 12.Aug.2019
%Description: Takes in the filename and from that generates a key to be
%used in the data struct.

function key = SIMSFieldnames(filename)
% %remove non-valid key characters
% key = strrep(filename, '_', '');
% key = strrep(key, ' ', '');
% key = strrep(key, '-', 'minus');
% key = strrep(key, '+', 'plus');
%
% %remove file extension
% key = strrep(key,'.xlsx', '');

key = '';
x = '';
process = 0;
iron = false;
minusSec = false;

%What repeat used?
index = find(filename == '_');
if numel(index) > 1
    x = filename(index(end)+1:index(end)+2);
end

%process order
%1: Anneal
%2: Non-Processed
%3: Standard
%4: Plasma
%5: Polished

%What process used?
if contains(filename,'nneal')
    process = 1;
elseif contains(filename,'roc')
    process = 2;
elseif contains(filename,'andard')|| contains(filename, 'Cal')
    process = 3;
elseif contains(filename,'plasma')
    process = 4;
elseif contains(filename,'polish')
    process = 5;
end

%Iron present?
if contains(filename, 'Fe')
    iron = true;
end
```

```
%Minus or Plus secondaries?
if contains(filename,'-sec')
    minusSec = true;
end

%Stitching together filename:
%process + iron + repeat + +/- ions

%process order
%1: Anneal
%2: Non-Processed
%3: Standard
%4: Plasma
%5: Polished
switch process
    case 1
       key = strcat(key,'Anneal');
    case 2
        key = strcat(key,'NonProcess');
    case 3
        key = strcat(key,'Standard');
    case 4
        key = strcat(key,'CNTplasma');
    case 5
        key = strcat(key,'CNTpolish');
    otherwise
        key = strcat(key,'processUnidentified');
end

%iron or no
if iron
    key = strcat(key,'Fe');
end

%What repeat
key = strcat(key,x);

%What Ions measured
if minusSec
    key = strcat(key,'minussec');
else
    key = strcat(key,'plussec');
end
end
```

rebinning.m:

```
%Title: rebinning.m
%Author: Berg Dodson
%Version: 1
%Date: 12.Aug.2019
%input: data(Contains the relavent data, 2D column arranged matrix),
%binStep(number in nm of how large the reformatted depthstep will be,
%double)
%Description: Takes an array of data pairs and a new bin step (units of
%independent var) and creates a reformatted array that has the modified bin
%step in independent variable and distributes the counts from the passed
%data appropriately

function reformatted = rebinning(data, binStep)
%Collecting the binstepfor data to be reformated
tempBinStep = data(3,1)- data(2,1);

%creating the array that will be passed back
reformatted = zeros(floor((data(end,1)./binStep)+1),2);

%Putting in the independent variable
reformatted(1:end,1) = 0:binStep:data(end,1);
% reformatted(end,1) = data(end,1);

%dumping counts into the dependant cells
%Var used to store the leftover counts from cells that are split on the
%edge of a depth step
remainder = 0;
for a = 1:length(reformatted)
    %cells to sum that fall within the current depth step
    %Since the checking condition is cells that are less than the value of
    %the next step, the cell that will be split is the last cell in the
    %range selected by this test
    stepArray = (data(:,1) >= reformatted(a,1))& ...
        (data(:,1) <= reformatted(a,1)+ binStep);
    reformatted(a,2) = sum(data(stepArray,2))+ remainder;
    remainder = 0;

    %Gets the indicies of the cells in the summing range
    check = find(stepArray);

    %check to see if the last cell in the range is split
    splitValue = reformatted(a,1)+ binStep;
%     check
    if data(check(end,1),1) ~= splitValue
        stepDiff = (splitValue - data(check(end,1),1));
        fraction = stepDiff/tempBinStep;
        remainder = (1-fraction)*data(check(end,1),2);
    end

%     remainder
    %adding the counts from the cells in the depth range
    reformatted(a,2) = reformatted(a,2) - remainder;
end
end
```

aluminumRatio.m:

```
%Title: aluminumRatio.m
%Author: Berg Dodson
%Version: 1
%Date: 9.Sept.2019
%input: fe(Contains the relavent data, 2D column arranged matrix[depth and
%counts]), al(Contains the relavent data, 2D column arranged matrix [depth
%and counts])Description: Takes the number of counts of al and fe at their
%corresponding depths and makes the ratio c/al for the alumina portion of
%the sample

function ratioList = aluminumRatio(c,al)

ratioList = zeros(size(c));
ratioList(:,1) = c(:,1);
ratioList(:,2) = c(:,2)./al(:,2);

end
```